Inorganic Chemistry
Article

Inorg. Chem. **2010**, *49*, 8045–8055 **8045**
DOI: 10.1021/ic1010693

Sulfur-Based Redox Reactions in $Mo_3S_7^{4+}$ and $Mo_3S_4^{4+}$ Clusters Bearing Halide and 1,2-Dithiolene Ligands: a Mass Spectrometric and Density Functional Theory Study

Rosa Llusar,[†] Victor Polo,[*,‡,§] Ederley Velez,[†] and Cristian Vicent[*,∥]

[†]*Departament de Química Física i Analítica, Universitat Jaume I, Av. Sos Baynat s/n, 12071 Castelló, Spain,* [‡]*Instituto de Biocomputación y Física de los Sistemas Complejos (BIFI), Edificio Cervantes, Corona de Aragón 42, Zaragoza 50009, Spain,* [§]*Departamento de Química Orgánica y Química Física, Universidad de Zaragoza, c/Pedro Cerbuna s/n, 50009 Zaragoza, Spain, and* [∥]*Serveis Centrals d'Instrumentació Científica, Universitat Jaume I, Avda. Sos Baynat s/n, E-12071, Castelló, Spain*

Received May 27, 2010

The gas phase fragmentation reactions of sulfur-rich $[Mo_3S_7Br_6]^{2-}$ ($\mathbf{1}^{2-}$), $[Mo_3S_7(bdt)_3]^{2-}$ ($\mathbf{2}^{2-}$), and $[Mo_3S_4(bdt)_3]^{2-}$ ($\mathbf{3}^{2-}$) (bdt = benzenedithiolate) complexes have been investigated by electrospray ionization (ESI) tandem mass spectrometry and theoretical calculations at the density functional theory level. Upon collision induced dissociation (CID) conditions, the brominated $\mathbf{1}^{2-}$ dianion dissociates through two sequential steps that involves a heterolytic Mo−Br cleavage to give $[Mo_3S_7Br_5]^-$ plus Br^- followed by a two-electron redox process that affords $[Mo_3S_5Br_5]^-$ and diatomic S_2 sulfur. Dianion $[Mo_3S_7(bdt)_3]^{2-}$ ($\mathbf{2}^{2-}$) dissociates through two sequential redox processes evolving diatomic S_2 sulfur and neutral bdt to yield $[Mo_3S_5(bdt)_3]^{2-}$ and $[Mo_3S_5(bdt)_2]^{2-}$, respectively. Conversely, dianion $[Mo_3S_4(bdt)_3]^{2-}$ ($\mathbf{3}^{2-}$), with sulfide instead of disulfide S_2^{2-} bridged ligands, remains intact under identical fragmentation conditions, thus highlighting the importance of disulfide ligands (S_2^{2-}) as electron reservoirs to trigger redox reactions. Regioselective incorporation of ^{34}S and Se at the equatorial position of the Mo_3S_7 cluster core in $\mathbf{1}^{2-}$ and $\mathbf{2}^{2-}$ have been used to identify the product ions along the fragmentation pathways. Reaction mechanisms for the gas-phase dissociation pathways have been elucidated by means of B3LYP calculations, and a comparison with the solution reactivity of Mo_3S_7 and Mo_3S_4 clusters as well as closely related Mo/S/dithiolene systems is also discussed.

Introduction

Group 6 transition metal sulfides are employed as catalyst for many industrial processes.[1] Coordination of bis(dithiolene) ligands to this class of compounds has expanded the scope to areas ranging from optical, conducting, and magnetic materials,[2] as well as in biological electron transport and enzyme-catalyzed reactions.[3] It is well documented that the redox versatility associated to group 6 dithiolene complexes is essential for many of these applications. Redox transformations involving group 6 metal, ligand-based processes, or an interplay between them, have been observed in mono- and dinuclear group 6 sulfide compounds, the extent of such electron transfer being typically system dependent.[4] Another type of electron transfer processes that dominates the group 6 chemistry of mono and dinuclear complexes is that occurring through simultaneous metal and ligand-based electron transfer reactions promoted by external oxidants. This represents the so-called induced internal redox reactions first identified by Stiefel et al.,[5,6] and whose relevance to the molybdenum and tungsten enzymes has been envisioned.[1,7] Internal induced redox processes are not exclusive of sulfur-rich group 6 complexes, and they has also been identified in a number of V/S/dithiolene[8] or Re/S/dithiolene complexes.[9]

Conversely to the mono- and dinuclear sulfur group 6 complexes, the redox chemistry of trinuclear Mo_3S_7 cluster

*To whom correspondence should be addressed. Fax: +34 976 761202 (V. P.), +34 964 387309 (C.V.). Phone: +34 976 761203 (V.P.), +34 964 387344 (C.V.). E-mail: vipolo@unizar.es (V.P.), barrera@sg.uji.es (C.V.).

(1) Stiefel, E. I. *Transition Metal Sulfur Chemistry: Biological and Industrial Significance*; Stiefel, E. I., Matsumoto, K., Eds.; American Chemical Society: Washington, DC, 1996; Vol. *653*, p 2.
(2) (a) Allen, A. E.; Olk, R. M. *Coord. Chem. Rev.* **1999**, *188*, 211. (b) Matsubayashi, G.; Nakano, M.; Tamura, H. *Coord. Chem. Rev.* **2002**, *226*, 143. (c) Faulmann, C.; Cassoux, P. *Prog. Inorg. Chem.* **2004**, *52*, 399. (d) Cummings, S. D.; Eisenberg, R. *Prog. Inorg. Chem.* **2004**, *52*, 315.
(3) (a) Hille, R. *Chem. Rev.* **1996**, *96*, 2757. (b) Johnson, M. K.; Rees, D. C.; Adams, M. W. W. *Chem. Rev.* **1996**, *96*, 2817. (c) McMaster, J.; Tunney, J. M.; Garner, C. D. *Prog. Inorg. Chem.* **2004**, *52*, 539.
(4) Young, C. G. *J. Inorg. Biochem.* **2007**, *101*, 1562.
(5) Coyle, C. L.; Harmer, M. A.; George, G. N.; Daage, M.; Stiefel, E. I. *Inorg. Chem.* **1990**, *29*, 14.
(6) Wang, K.; McConnachie, J. M.; Stiefel, E. I. *Inorg. Chem.* **1999**, *38*, 4334.
(7) Stiefel, E. I. *Pure Appl. Chem.* **1998**, *70*, 889.
(8) Halbert, T. R.; Hutchings, L. L.; Rhodes, R.; Stiefel, E. I. *J. Am. Chem. Soc.* **1986**, *108*, 6437.
(9) (a) Murray, H. H.; Wei, L.; Sherman, S. E.; Greaney, M. A.; Eriksen, K. A.; Carstensen, B.; Halbert, T. R.; Stiefel, E. I. *Inorg. Chem.* **1995**, *34*, 841. (b) McConnachie, C. A.; Stiefel, E. I. *Inorg. Chem.* **1999**, *38*, 964. (c) Dessapt, R.; Simonnet-Jégat, C.; Riedel, S.; Marrot, J.; Secheresse, F. *Trans. Met. Chem.* **2002**, *27*, 234.

Published on Web 08/09/2010

Scheme 1

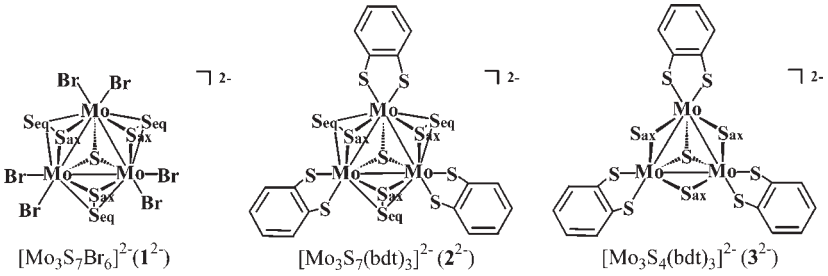

$[Mo_3S_7Br_6]^{2-}$ ($\mathbf{1}^{2-}$) $[Mo_3S_7(bdt)_3]^{2-}$ ($\mathbf{2}^{2-}$) $[Mo_3S_4(bdt)_3]^{2-}$ ($\mathbf{3}^{2-}$)

complexes involves exclusively the sulfur ligands where the Mo centers are mere spectators. Hence, reduction of Mo_3S_7 clusters proceeds through μ-S_2 to μ-S transformation to afford the corresponding Mo_3S_4 complexes. As far as the oxidation behavior of the Mo_3S_7 clusters is concerned, we have recently shown that coordination of bis(dithiolenes) to Mo_3S_7 clusters provides oxidation activity suggesting a dominant contribution of the dithiolene ligand to the highest occupied molecular orbital (HOMO) of the Mo_3S_7/dithiolene cluster complex.[10−12]

The understanding of electron transfer reactions involving group 6/sulfide/dithiolene complexes is crucial to anticipate the preferred redox pathway of the target species and therefore to control the products formed as well as their yields. For example, the mechanism of the induced redox reaction between MoS_4^{2-} and organic disulfides have been elucidated providing valuable clues to the rational preparation of new lower valent group 6 sulfur-containing species.[5,13] However, investigating electron transfer processes at the molecular level remains a task of great complexity, mainly because of the transient nature of the intermediates involved, the concerted nature of the process, or the presence of side reactions. One way to address the mechanistic elucidation of a chemical process at the molecular level consists in paralleling the chemical process observed both in solution and solid state, in a well-defined gas-phase environment in which solvent, counteranions, aggregation processes, or side reactions are absent making the study much simpler. In this context, tandem mass-spectrometric methods in conjunction with theoretical calculations have proved useful in elucidating mechanistic aspects.[14,15] In particular, electrospray ionization mass spectrometry (ESI-MS) and its tandem version have become increasingly popular as an analytical tool in inorganic and organometallic chemistry because it allows pre-existing molecules in solution to be gently transferred to the gas-phase.[15,16] For example, gas-phase generation and reactivity and photoelectron spectroscopy studies of ESI-generated group 6 oxides[17] or group 6/dithiolene complexes have extensively investigated.[18,19]

Herein, we report an experimental study on the gas-phase production and the fragmentation reactions of group 6 sulfides featuring Mo_3S_7 and Mo_3S_4 cluster cores (see Scheme 1) using ESI and ESI tandem mass spectrometry. C_3-symmetrized trinuclear Mo_3S_7 clusters constitute a large family of inorganic compounds in which the cluster core is coordinated to a wide spectrum of ligands with applications in multidisciplinary fields.[20] Mo_3S_7 clusters present an equilateral Mo_3 triangular core capped by a μ_3-S atom that lies above the metal plane as illustrated in Scheme 1. Additionally, three bridging μ-S_2 groups or μ-S_{ax} groups connect adjacent metal atoms, with three sulfur atoms occupying equatorial positions (S_{eq}, essentially in the Mo_3 plane), and three axial sulfur atoms (S_{ax}, located out of the metal plane) on opposite sides to that of the μ_3-S capping atom. In addition, the study of trinuclear Mo_3S_9 molybdenum clusters is also motivated by their putative presence as intermediates during catalytic MoS_x-based hydrodesulfurization reactions, this Mo_3S_9 unit being a widely

(10) Garriga, J. M.; Llusar, R.; Uriel, S.; Vicent, C.; Usher, A. J.; Lucas, N. T.; Humphrey, M. G.; Samoc, M. *Dalton Trans*. **2003**, 4546.
(11) (a) Llusar, R.; Uriel, S.; Vicent, C.; Coronado, E.; Gomez-Garcia, C. J.; Clemente-Juan, J. M.; Braida, B.; Canadell, E. *J. Am. Chem. Soc*. **2004**, *126*, 12076. (b) Alberola, A.; Llusar, R.; Triguero, S.; Vicent, C.; Sokolov, M. N.; Gómez-Garcia, C. *J. Mater. Chem*. **2007**, *17*, 3440.
(12) Llusar, R.; Triguero, S.; Polo, V.; Vicent, C.; Gomez-Garcia, C.; Jeannin, O.; Fourmigue, M. *Inorg. Chem*. **2008**, *47*, 9400.
(13) Harmer, M. A.; Halbert, T. R.; Pan, W.-H.; Coyle, C. L.; Cohen, S. A.; Stiefel, E. I. *Polyhedron* **1986**, *5*, 341.
(14) (a) Alcami, M.; Mo, O.; Yañez, M. *Mass Spectrom. Rev*. **2001**, *20*, 195. (b) Armentrout, P. B. *Int. J. Mass Spectrom*. **2003**, *227*, 289. (c) Bohme, D. K.; Schwarz, H. *Angew. Chem., Int. Ed*. **2005**, *44*, 2336. (d) Schröder, D.; Schwarz, H. *Top. Organomet. Chem*. **2007**, *22*, 1. (e) Johnson, G. E.; Tyo, E. C.; Castleman, J., A. W. *Proc. Natl. Acad. Sci. U.S.A*. **2008**, *105*, 18108. (f) Johnson, G. E.; Mitric, R.; Bonacic-Koutecky, V.; Castleman, A. W., Jr. *Chem. Phys. Lett*. **2009**, *475*, 1. (g) Roithova, J.; Schröder, D. *Coord. Chem. Rev*. **2009**, *253*, 666. (h) Roithova, J.; Schröder, D. *Chem. Rev*. **2010**, *110*, 1170.
(15) O'Hair, R. A. J. *Chem. Commun* **2006**, 1469.
(16) (a) Chen, P. *Angew. Chem., Int. Ed*. **2003**, *42*, 2832. (b) Bernhardt, T. M. *Int. J. Mass Spectrom*. **2005**, *243*, 1.
(17) (a) Waters, T.; O'Hair, R. A. J.; Wedd, A. G. *J. Am. Chem. Soc*. **2003**, *125*, 3384. (b) Feyel, S.; Waters, T.; O'Hair, R. A. J.; Wedd, A. G. *Dalton Trans*. **2004**, 4010. (c) Yang, X.; Waters, T.; Wang, X. B.; O'Hair, R. A. J.; Wedd, A. G.; Dixon, D. A.; Wang, L. S. *J. Phys. Chem. A* **2004**, *108*, 10089. (d) Waters, T.; O'Hair, R. A. J.; Wedd, A. G. *Inorg. Chem*. **2005**, *44*, 3356. (e) Zhai, H. J.; Huang, X.; Waters, T.; Wang, X. B.; O'Hair, R. A. J.; Wedd, A. G.; Wang, L. S. *J. Phys. Chem. A* **2005**, *109*, 10512. (f) Waters, T.; Wang, X. B.; Li, S. G.; Kiran, B.; Dixon, D. A.; Wang, L. S. *J. Phys. Chem. A* **2005**, *109*, 11771. (g) Waters, T.; Huang, X.; Wang, X. B.; Woo, H. K.; O'Hair, R. A. J.; Wedd, A. G.; Wang, L. S. *J. Phys. Chem. A* **2006**, *110*, 10737. (h) Vicent, C.; Feliz, M.; Llusar, R. *J. Phys. Chem. A* **2008**, *112*, 12550. (i) Llusar, R.; Sorribes, I.; Vicent, C. *J. Clust. Sci*. **2009**, *20*, 177. (j) Ma, M. T.; Waters, T.; Beyer, K.; Palamarczuk, R.; Richardt, P. J. S.; O'Hair, R. A. J.; Wedd, A. G. *Inorg. Chem*. **2009**, *48*, 598. (k) Vila-Nadal, L.; Rodriguez-Fortea, A.; Yan, L. K.; Wilson, E. F.; Cronin, L.; Poblet, J. M. *Angew. Chem., Int. Ed*. **2009**, *48*, 5452.
(18) (a) Dessapt, R.; Simonnet-Jegat, C.; Mallard, A.; Lavanant, H.; Marrot, J.; Secheresse, F. *Inorg. Chem*. **2003**, *42*, 6425. (b) Waters, T.; Blanksby, S. J.; Zhang, L. Y.; O'Hair, R. A. J. *Org. Biomol. Chem*. **2004**, *2*, 190. (c) Waters, T.; Wang, X. B.; Yang, X.; Zhang, L.; O'Hair, R. A. J.; Wang, L. S.; Wedd, A. G. *J. Am. Chem. Soc*. **2004**, *126*, 5119. (d) Lavanant, H.; Fressigne, C.; Simonnet-Jegat, C.; Dessapt, R.; Mallard, A.; Secheresse, F.; Sellier, N. *Int. J. Mass Spectrom*. **2005**, *243*, 205.
(19) Llusar, R.; Triguero, S.; Vicent, C.; Sokolov, M. N.; Domercq, B.; Fourmigue, M. *Inorg. Chem*. **2005**, *44*, 8937.
(20) (a) Sakane, G.; Shibahara, T. *Transition Metal Sulfur Chemistry: Biological and Industrial Significance*; Stiefel, E. I., Matsumoto, K., Eds.; American Chemical Society: Washington, DC, 1996; Vol. *653*, p 225; (b) Saito, T. *Adv. Inorg. Chem*. **1997**, *44*, 45. (c) Llusar, R.; Vicent, C. *Trinuclear Molybdenum and Tungsten Cluster Chalcogenides: From Solid State to Molecular Materials. Inorganic Chemistry in Focus III*; Meyer, G.; Naumann, D., Wesemann, L., Eds.; Wiley-VCH Verlag: Weinheim, Germany, 2006; p 105; (d) Fedorov, V. E.; Mironov, Y. V.; Naumov, N. G.; Sokolov, M. N.; Fedin, V. P. *Russ. Chem. Rev*. **2007**, *76*, 529. (e) Llusar, R.; Vicent, C. *Coord. Chem. Rev*. **2010**, *254*, 1534.

investigated molecular model to reproduce the periodicity of the bulk MoS_3 solid.[21] For the $[Mo_3S_7Br_6]^{2-}$ ($\mathbf{1}^{2-}$) and $[Mo_3S_7(bdt)_3]^{2-}$ ($\mathbf{2}^{2-}$) (bdt = 1,2-benzenedithiolate) dianions investigated in this work, the outer groups (Br or bdt) fill the remaining two positions. In $[Mo_3S_4(bdt)_3]^{2-}$ ($\mathbf{3}^{2-}$), the equatorial atoms are missing and 1,2-benzenedithiolate ligands complete the Mo environment. We have chosen these $\mathbf{1}^{2-}$-$\mathbf{3}^{2-}$ dianions as models to systematically analyze the effects that modification of the inner bridged ligand (S_2^{2-} or S^{2-}) and the peripheral ligand (Br or bdt) have on the identity of the formed product ions upon gas-phase fragmentation conditions.

The fragments evolved (neutral S_2 and the dithiete bdt) upon collision induced dissociation (CID) conditions formally correspond to oxidation products concomitant with Mo_3S_7 cluster reduction whose energetic profiles are rationalized on the basis of complementary isotopically ^{34}S labeling experiments and density functional theory (DFT) calculations.

Experimental Section

General Procedures. All reactions were carried out under a nitrogen atmosphere using standard Schlenk techniques. Isotopically labeled $^{34}SPPh_3$ was prepared starting from PPh_3 and elemental $^{34}S_8$ (99.5% ^{34}S, Sigma-Aldrich) and characterized by ^1H, ^{13}C, and $^{31}P\{^1H\}$NMR.[22] The ESI mass spectrum of CH_2Cl_2:CH_3OH solutions $^{34}SPPh_3$ reveals the presence of a prominent peak attributed to the $[^{34}SPPh_3+H]^+$ (m/z = 297) adduct. Compounds $(n\text{-}Bu_4N)_2[Mo_3S_7Br_6]$ ($(n\text{-}Bu_4N)_2[\mathbf{1}]$),[23] $(n\text{-}Bu_4N)_2[Mo_3S_4Se_3Br_6]$,[24] and $(n\text{-}Bu_4N)_2[Mo_3S_7(bdt)_3]$ ($(n\text{-}Bu_4N)_2[\mathbf{2}]$),[12] were prepared according to literature methods. Regioselective ^{34}S isotopic labeling at the equatorial positions in Mo_3S_7 clusters has been previously reported.[23,25] For compounds $(n\text{-}Bu_4N)_2[\mathbf{1}]$ and $(n\text{-}Bu_4N)_2[\mathbf{2}]$ we follow a modification which consists in refluxing these complexes with a 10-fold excess of $^{34}SPPh_3$ in acetonitrile for 1 h. The $[Mo_3S_4Se_3(bdt)_3]^{2-}$ dianion was prepared by stirring acetonitrile solutions of $[Mo_3S_4Se_3Br_6]^{2-}$, a 5-fold excess of the 1,2-benzenedithiol and triethylamine for 1 h and subsequently transferred to the gas-phase by ESI. The remaining reactants were obtained from commercial sources and used as received. Solvents for synthesis were dried and degassed by standard methods before use. Elemental analysis was performed on an EA 1108 CHNS microanalyzer. IR spectra were recorded on a Perkin-Elmer System 2000 FT-IR using KBr pellets. Cyclic voltammetry experiments were performed in CH_3CN with an Echochemie Pgstat 20 electrochemical analyzer and a conventional three-electrode configuration consisting of platinum working and auxiliary electrodes and a Ag/AgCl reference electrode.

Synthesis. **$(n\text{-}Bu_4N)_2[Mo_3S_4(bdt)_3]$ ($(n\text{-}Bu_4N)_2[\mathbf{3}]$).** PPh_3 (0.03 g, 0.11 mmol.) was added to a red solution of $(n\text{-}Bu_4N)_2[Mo_3S_7(bdt)_3]$ ($(n\text{-}Bu_4N)_2[\mathbf{2}]$) (0.05 g, 0.03 mmol) in 10 mL of acetonitrile under nitrogen. The solution was stirred for 10 min, and the desired compound $(n\text{-}Bu_4N)_2[\mathbf{3}]$ was precipitated with diethylether. The precipitate was separated from the solution by filtration under inert atmosphere, washed thoroughly with toluene and diethylether to eliminate the PPh_3S, and recrystallized from CH_2Cl_2/diethylether mixtures. (0.024 g, 52%). (Found: C, 33.03; H 4.96, S 40.97, N 1.92. $Mo_3S_{19}C_{41}H_{72}N_2$ requires C 33.05, H 4.87, S 40.88, N 1.88). IR (KBr) cm^{-1}: 1459 (s), ν(C=C); 1054 (vs), ν(C=S); 512 (m), ν(C−S); 469 (m), ν(Mo−S_{bdt}) and ν(Mo-(μ-S)); ESI-MS(-) m/z: 503 $[M]^{2-}$.

X-ray Studies. Cation exchange in compound $(n\text{-}Bu_4N)_2[\mathbf{3}]$ was carried out by adding an excess of PPh_4Br in acetonitrile that precipitates the desired $(PPh_4)_2[\mathbf{3}]$ compound. Suitable crystals for X-ray studies for compound $(PPh_4)_2[\mathbf{3}]$ were grown by slow diffusion of diethylether into sample solutions in CH_2Cl_2 under rigorous inert atmosphere. The data collection was performed on a Bruker Smart CCD diffractometer using graphite-monochromated Mo Kα radiation (λ = 0.71073 Å). A hemisphere of data was collected based on three ω-scans runs (starting $\omega = -28°$) at values $\phi = 0°$, 90°, and 180° with the detector at $2\theta = 28°$. At each of these runs, frames (606, 435, and 230 respectively) were collected at 0.3° intervals and 35 s per frame. The diffraction frames were integrated using the SAINT package and corrected for absorption with SADABS.[26] The positions of the heavy atoms were determined by direct methods and successive difference electron density maps using the SHELXTL 5.10 software package were done to locate the remaining atoms.[27] Refinement was performed by the full-matrix-least-squares method based on F^2. All atoms in compound $(PPh_4)_2[\mathbf{3}]$ were refined anisotropically. All hydrogen atoms of the phenyl groups were generated geometrically. Crystal data for $(PPh_4)_2[\mathbf{3}]$: $C_{66}H_{52}Mo_3P_2S_{10}$, M = 1515.44, monoclinic, space group Cc, a = 13.020(2), b = 23.573(4), c = 21.833(3), β = 106.805(4), V = 6415(2) Å^3, T = 293 K, Z = 4, $\mu(Mo_{K\alpha})$ = 0.993 mm^{-1}. Reflections collected/unique = 18024/8402 (R_{int} = 0.1326). Final refinement converged with R_1 = 0.0719 for 7305 reflections with $F_0 \geq 4\sigma(F_0)$ and wR_2 = 0.1866 for all reflections, GoF = 1.005, max/min residual electron density 1.032/−1.697 e·Å^{-3}.

ESI Mass Spectrometry. A hybrid QTOF I (quadrupole-hexapole-TOF) mass spectrometer with an orthogonal Z-spray-electrospray interface (Waters, Manchester, U.K.) was used. The desolvation gas as well as nebulizing gas was nitrogen at a flow of 800 L/h and 20 L/h respectively. The temperature of the source block was set to 120 °C and the desolvation temperature to 150 °C. Mass calibration was performed using a solution of sodium iodide in isopropanol/water (50:50) from m/z 100 to 1900. A capillary voltage of 3.3 KV was used in the negative scan mode, and the cone voltage was set to 10 V to control the extent of fragmentation of the identified ions. Sample solutions were infused via syringe pump directly connected to the ESI source at a flow rate of 10 μL/min. The observed isotopic pattern of each intermediate perfectly matched the theoretical isotope pattern calculated from their elemental composition using the MassLynx 4.0 program. Tandem MS/MS spectra were obtained at various collision energies (typically varied from E_{lab} 0−50 eV) by selecting the precursor ion of interest with the first quadrupole (Q1) and scanning with the time-of-flight analyzer (TOF). The complete envelope of each ion was mass-selected except for samples enriched with ^{34}S for which a single isotopomer was mass-selected. Argon was used as a collision gas to produce the pressure of 3×10^{-5} mbar as measured in the quadrupole analyzer region.

Computational Details. All calculations were carried out using the Gaussian03 program.[28] The commonly used B3LYP functional[29] is employed in combination with the 6-31G(d,p) basis set for S, Br, C, and H atoms[30] and the effective core

(21) (a) Jiao, H.; Li, Y.-W.; Delmon, B.; Halet, J.-F. *J. Am. Chem. Soc.* **2001**, *123*, 7334. (b) Yao, X.-Q.; Li, Y.-W.; Jiao, H. *J. Mol. Struct. TEOCHEM* **2005**, *726*, 67. (c) Yao, X.-Q.; Li, Y.-W.; Jiao, H. *J. Mol. Struct. TEOCHEM* **2005**, *726*, 81. (d) Zeng, T.; Wen, X.-D.; Li, Y.-W.; Jiao, H. *J. Phys. Chem. B* **2005**, *109*, 13704. (e) Murugan, P.; Kumar, V.; Kawazoe, Y.; Ota, N. *J. Phys. Chem. A* **2007**, *111*, 2778.

(22) Tkachenko, S. E.; Trofimova, T. P.; Fedoseev, V. M. *Chem. Heterocycl. Compd.* **1999**, *35*, 973.

(23) Fedin, V. P.; Sokolov, M. N.; Mironov, Y. V.; Kolesov, B. A.; Tkachev, S. V.; Fedorov, V. Y. *Inorg. Chim. Acta* **1990**, *167*, 39.

(24) Fedin, V. P.; Mironov, Y. V.; Sokolov, M. N.; Kolesov, B. A.; Fedorov, V. Y.; Yufit, D. S.; Struchkov, Y. T. *Inorg. Chim. Acta* **1990**, *174*, 275.

(25) Fedin, V. P.; Kolesov, B. A.; Mironov, Y. V.; Fedorov, V. Y. *Polyhedron* **1989**, *8*, 2419.

(26) (a) *SAINT*, version 6.2; Bruker Analytical X-Ray Systems: Madison, WI, 2001; (b) Sheldrick, G. M. *SADABS, empirical absorption program*; University of Göttingen: Göttingen, Germany, 2001.

(27) Sheldrick, G. M. *SHELXTL*, version 5.1; Bruker Analytical X-Ray Systems: Madison, WI, 1997.

(28) Frisch, M. J. et al. *Gaussian03*, revision C.02; Gaussian,Inc.: Wallingford, CT, 2003.

(29) (a) Becke, A. D. *Phys. Rev. A.* **1988**, *38*, 3098. (b) Lee, C. T.; Yang, W. T.; Parr, R. G. *Phys. Rev. B* **1988**, *37*, 785. (c) Becke, A. D. *J. Chem. Phys.* **1993**, *98*, 1372.

(30) Hehre, W. J.; Ditchfield, R.; Pople, J. A. *J. Chem. Phys.* **1972**, *56*, 2257.

potentials (ECP) of Stuttgart RSC 1993 on Mo atoms.[31] Full geometry optimizations were performed followed by analytical calculation of frequencies to determine the nature of the stationary point.

Results and Discussion

Compounds $(n\text{-}NBu_4)_2$[**1**] and $(n\text{-}NBu_4)_2$[**2**] are accessed starting from the preassembled molecular $(NH_4)_2[Mo_3S_{13}]$ complex.[12,23] Complex $(n\text{-}Bu_4N)_2[Mo_3S_4(bdt)_3]$ ($(n\text{-}Bu_4N)_2$[**3**]) featuring a Mo_3S_4 core can be easily obtained by treatment of acetonitrile solutions of $(n\text{-}Bu_4N)_2$[**2**] with 3 equiv of triphenylphosphine according to eq 1.

$$[Mo_3S_7(bdt)_3]^{2-} + 3PPh_3 \rightarrow [Mo_3S_4(bdt)_3]^{2-} + 3SPPh_3 \quad (1)$$

Compound $(n\text{-}Bu_4N)_2$[**3**] has been characterized by IR spectroscopy, ESI mass spectrometry, and X-ray single crystal analysis. An Oak Ridge thermal ellipsoid plot (ORTEP) diagram of the $\mathbf{3}^{2-}$ dianion is shown in the Supporting Information, Figure S1. As pointed out above, the redox chemistry of compounds $(n\text{-}Bu_4N)_2$[**1**] and $(n\text{-}Bu_4N)_2$[**2**] is dominated by reduction processes assigned to the sulfur-based reduction $Mo_3S_7 \rightarrow Mo_3S_4$ (formal reduction of the three disulfide-bridged ligands to three sulfide-bridged ligands).[10,32] Replacement of bromine terminal atoms ($[\mathbf{1}]^{2-}$) by the organic bdt ($[\mathbf{2}]^{2-}$) results in a dramatic change in the electrochemical features, compound $(n\text{-}Bu_4N)_2$[**2**] displaying two quasireversible oxidation waves at easily accessible potentials $E_{1/2} = 0.23$ V ($\Delta E = 70$ meV) and $E_{1/2} = 0.41$ V ($\Delta E = 120$ meV) which are assigned to dithiolene-based oxidation processes. Compound $(n\text{-}Bu_4N)_2$[**3**] with a Mo_3S_4 also shows two oxidation waves (see Supporting Information, Figure S2) at potentials $E^0 = 0.47$ V and $E^0 = 0.65$ V versus Ag/AgCl (not observed in other Mo_3S_4 clusters), thus indicating a contribution from the dithiolene ligand to the HOMO orbital of the Mo_3S_4 cluster core. Cyclic voltammetry experiments clearly indicate that redox chemistry of trinuclear Mo_3S_7 (or Mo_3S_4)/dithiolene complexes is dominated by ligand-based processes where the Mo atoms are essentially spectators.

Gas-Phase Fragmentation Reactions of the $\mathbf{1}^{2-}$, $\mathbf{2}^{2-}$, and $\mathbf{3}^{2-}$ Dianions. The ESI mass spectra of compounds $(n\text{-}Bu_4N)_2$[**1**], $(n\text{-}Bu_4N)_2$[**2**], and $(n\text{-}Bu_4N)_2$[**3**] recorded under soft ionization conditions (that means low U_c cone voltages),[33] show the corresponding doubly charged $\mathbf{1}^{2-}$, $\mathbf{2}^{2-}$, and $\mathbf{3}^{2-}$ ions as base peaks. The ESI mass spectrum of compound $(n\text{-}Bu_4N)_2$[**1**] also revealed the presence of the singly charged $[\mathbf{1} - Br]^-$ species (ca. 40% with respect to the base peak) under our experimental conditions. The use of mass spectrometric techniques for the characterization of Mo_3S_7 complexes was first reported by Hegetschweiler et al. using fast atom bombardment (FAB) and liquid secondary ion mass spectrometry (L-SIMS) as ionization sources.[34,35] Laser vaporization techniques have also been used to produce $[Mo_3S_7]^+$ and $[Mo_3S_7]^-$ gas-phase ions.[36] A comparison of the identity of the ions generated using these different ionization sources reveals that only ESI allows the transfer of the intact transfer of dianions from the condensed to the gas-phase, in agreement with its inherent softer ionization character. For example, the FAB mass spectra of the dianionic $[Mo_3S_7(catecholate)_3]^{2-}$ complex show the presence of species of general formula $[Mo_3S_x(catecholate)_y]^-$ ($x = 4-7$, $y = 1-3$) because of an electron-detachment process together with partial release of sulfur and outer ligands.[34,35] To examine the gas-phase fragmentation reactions of dianions $\mathbf{1}^{2-}$, $\mathbf{2}^{2-}$, and $\mathbf{3}^{2-}$, the doubly charged species were mass selected and allowed to collide with argon in the collision cell. CID mass spectra of the $\mathbf{1}^{2-}$ dianion are shown in Figure 1. Fragmentation paths are schematized in eqs 2 and 3.

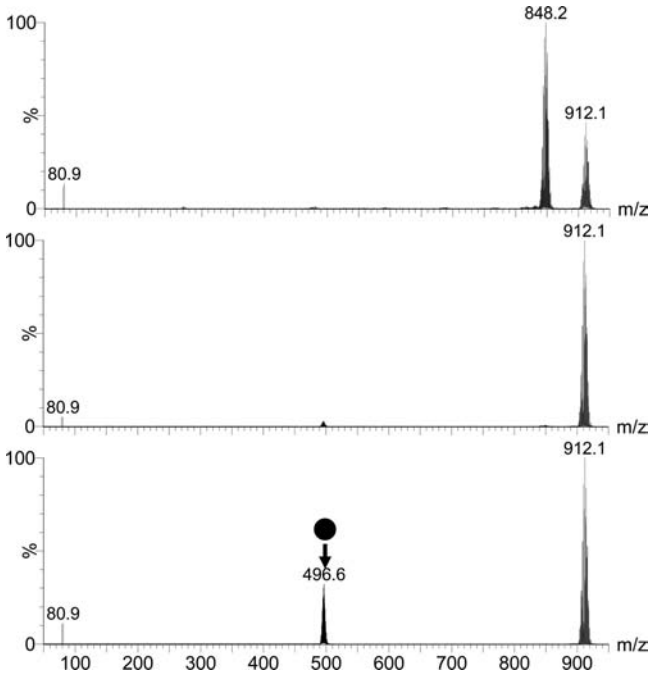

Figure 1. CID mass spectra of the $\mathbf{1}^{2-}$ ($m/z = 496.6$) dianion at increasing E_{lab} collision energies $E_{lab} = 10$ eV (bottom), $E_{lab} = 15$ eV (middle), and $E_{lab} = 20$ eV (top).

$$[Mo_3S_7Br_6]^{2-}\ (\mathbf{1}^{2-}) \rightarrow [Mo_3S_7Br_5]^-\ (\mathbf{1a}^-) + Br^- \quad (2)$$

$$[Mo_3S_7Br_5]^-\ (\mathbf{1a}^-) \rightarrow [Mo_3S_5Br_5]^-\ (\mathbf{1b}^-) + S_2 \quad (3)$$

The fragmentation channel depicted in eq 2 corresponds to the heterolytic cleavage of a Mo−Br bond to afford $[Mo_3S_7Br_5]^-$ ($\mathbf{1a}^-$) at $m/z = 912.1$ and the Br^- anion. This dissociation step was also anticipated from single-stage ESI mass spectrum of compound $(n\text{-}Bu_4N)_2$[**1**] for which $\mathbf{1}^{2-}$ and $\mathbf{1a}^-$ are the dominant species observed at relatively low ionization conditions (typically $U_c = 10$ V). The $\mathbf{1a}^-$ anion further dissociates by loss of neutral S_2 leading to the $[Mo_3S_5Br_5]^-$

(31) Dolg, M.; Stoll, H.; Preuss, H.; Pitzer, R. M. *J. Phys. Chem.* **1993**, *97*, 5852.
(32) Zimmermann, H.; Hegetschweiler, K.; Keller, T.; Gramlich, V.; Schmalle, H. W.; Petter, W.; Schneider, W. *Inorg. Chem.* **1991**, *30*, 4336.
(33) Cech, N. B.; Enke, C. G. *Mass Spectrom. Rev.* **2001**, *20*, 362.
(34) Hegetschweiler, K.; Keller, T.; Amrein, W.; Schneider, W. *Inorg. Chem.* **1991**, *30*, 873.
(35) Hegetschweiler, K.; Caravatti, P.; Fedin, V. P.; Sokolov, M. N. *Helv. Chim. Acta* **1992**, *75*, 1659.
(36) (a) Lightstone, J. M.; Mann, H. A.; Wu, M.; Johnson, P. M.; White, M. G. *J. Phys. Chem. B* **2003**, *107*, 10359. (b) Lightstone, J. M.; Patterson, M. J.; White, M. G. *Chem. Phys. Lett.* **2005**, *413*, 429. (c) Gemming, S.; Tamuliene, J.; Seifert, G.; Bertram, N.; Kim, Y. D.; Ganteför, G. *Appl. Phys. A: Mater. Sci. Process.* **2006**, *82*, 161. (d) Patterson, M. J.; Lightstone, J. M.; White, M. G. *J. Phys. Chem. A* **2008**, *112*, 12011.

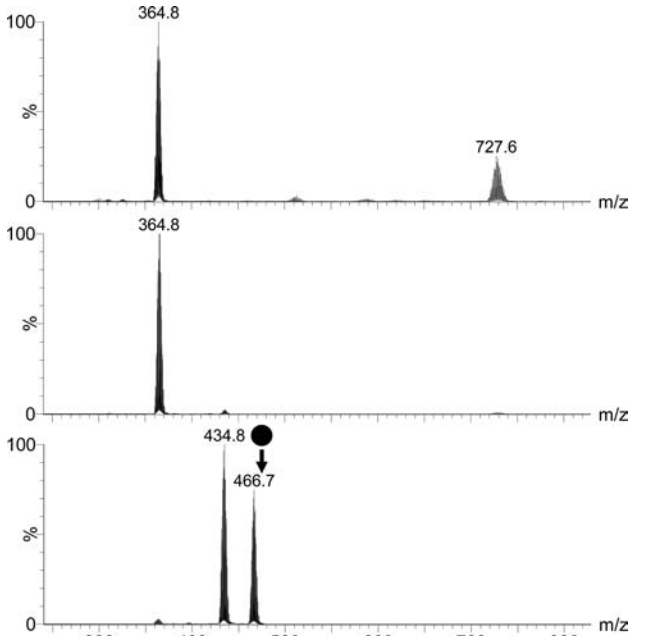

Figure 2. CID mass spectra of the $\mathbf{2}^{2-}$ (m/z = 466.7) dianion at increasing E_{lab} collision energies E_{lab} = 10 eV (bottom), E_{lab} = 20 eV (middle), and E_{lab} = 30 eV (top).

species at m/z = 848.2. CID mass spectra of the $\mathbf{2}^{2-}$ dianion are shown in Figure 2. Reactions 4, 5, and 6 depict its fragmentation paths.

$$[Mo_3S_7(bdt)_3]^{2-}\ (\mathbf{2}^{2-}) \rightarrow [Mo_3S_5(bdt)_3]^{2-}\ (\mathbf{2a}^{2-}) + S_2 \quad (4)$$

$$[Mo_3S_5(bdt)_3]^{2-}\ (\mathbf{2a}^{2-}) \rightarrow [Mo_3S_5(bdt)_2]^{2-}\ (\mathbf{2b}^{2-}) + bdt \quad (5)$$

$$[Mo_3S_5(bdt)_2]^{2-}\ (\mathbf{2b}^{2-}) \rightarrow [Mo_3S_5(bdt)_2]^{-}\ (\mathbf{2b}^{-}) + e- \quad (6)$$

For the $\mathbf{2}^{2-}$ dianion, the loss of S_2 (eq 4) leads to the dianion of formula $[Mo_3S_5(bdt)_3]^{2-}$ ($\mathbf{2a}^{2-}$) at m/z = 434.8 in a similar way to that observed for the $\mathbf{1a}^{-}$ anion (see eq 3), except that lower E_{lab} collision energies are required to liberate S_2 from the $\mathbf{2}^{2-}$ dianion in comparison with $\mathbf{1a}^{-}$. Increasing the collision energy up to E_{lab} = 30 eV results in the liberation of the neutral dithiete bdt (eq 5) to give the $[Mo_3S_5(bdt)_2]^{2-}$ specie at m/z = 364.8 together with a minor fragmentation channel that consists in a one-electron detachment step to afford the $[Mo_3S_5(bdt)_2]^{-}$ anion at m/z = 727.6 (eq 6). The CID spectra of the $\mathbf{3}^{2-}$ dianion recorded under identical conditions only reveal a minor fragmentation channel at high collision energies (typically E_{lab} 60 eV), which consist in a one-electron detachment process to afford the $\mathbf{3}^{-}$ anion.

$$[Mo_3S_4(bdt)_3]^{2-}\ (\mathbf{3}^{2-}) \rightarrow [Mo_3S_4(bdt)_3]^{-}\ (\mathbf{3}^{-}) + e- \quad (7)$$

As far as the identity of the product ions formed through processes depicted in eqs 1−6 is concerned, a number of isomers can be envisioned depending on the S atoms involved in the dissociations. For example, the expulsion of diatomic S_2 might come from rearrangement processes within the Mo_3S_7 cluster core to actually evolve two equatorial, two axial or mixed equatorial-axial sulfur atoms (the possibility of evolving the capping μ_3-S atom is not considered because of its well-documented inertness).[37] To account for the type of sulfur evolved, CID spectra of isotopically ^{34}S labeled and Se analogues have been investigated in combination with reliable quantum chemical calculations as detailed in the next section.

Regioselective ^{34}S Isotopic Labeled $Mo_3(\mu_3\text{-}S)(S_{ax})_3(^{34}S_{eq})_3$ and Se Homologues $Mo_3(\mu_3\text{-}S)(S_{ax})_3(Se_{eq})_3$. After treating acetonitrile solutions of $\mathbf{1}^{2-}$ and $\mathbf{2}^{2-}$ with $^{34}SPPh_3$ for one hour (see Experimental Section), the ESI mass spectra reveal prominent doubly charged species centered at m/z values slight shifted to higher values with respect to the $\mathbf{1}^{2-}$ and $\mathbf{2}^{2-}$ dianions in agreement with the occurrence of the ^{34}S enrichment on the Mo_3S_7 core at the equatorial positions.[23] Figure 3 a) shows the ESI mass spectrum of the reaction mixture of $[Mo_3S_7Br_6]^{2-}$ and $^{34}SPPh_3$ in the m/z = 900 to 935 region.

As can be inferred from Figure 3a, partial ^{34}S enrichment at the equatorial sites of $\mathbf{1}^{2-}$ has occurred as manifested by the mass gain of about 4 Da (note that complete ^{34}S incorporation at the S_{eq} would give rise to a cluster peak centered at m/z = 918 for $[1 - Br]^{-}$ while ^{34}S incorporation at both equatorial and axial positions would afford a peak centered at m/z = 924). According to this, liberation of a mixture of isotopically labeled S_2 neutral molecules is expected upon CID conditions where neutral $^{34}S^{32}S$ should predominate over $^{34}S_2$ and $^{32}S_2$. CID mass spectra (Figure 3 b) of mass-selected 916 reveal losses of 64, 66, and 68 associated to $^{32}S_2$, $^{32}S^{34}S$, and $^{34}S_2$, where liberation of neutral $^{32}S^{34}S$ is dominant, thus indicating that equatorial sulfur atoms are released in the fragmentation reactions depicted in eq 3 and 4. We also faced the study of chemical analogues to further validate the preferred involvement of the equatorial chalcogen atoms upon CID conditions. Hence, the $[Mo_3S_4Se_3Br_6]^{2-}$ and $[Mo_3S_4Se_3(bdt)_3]^{2-}$ species, where the equatorial positions are occupied by selenium, were also gas-phase generated and subjected to CID. CID spectra of $[Mo_3S_4Se_3Br_6]^{2-}$ and $[Mo_3S_4Se_3(bdt)_3]^{2-}$ were identical to that of $\mathbf{1}^{2-}$ and $\mathbf{2}^{2-}$ (see Supporting Information, Figure S3 for the $[Mo_3S_4Se_3Br_6]^{2-}$ dianion) except that diatomic Se_2 molecules are exclusively released, thus supporting that equatorial chalcogen atoms are invariably evolved in the CID spectra of Mo_3Q_7 (Q = S, Se) clusters.[34,35]

Determination of the Elementary Steps along the Dissociation Pathways Using Quantum Chemical Calculations. Full geometry optimizations using the B3LYP approach and a 6-31G(d,p) basis set for S, Br, C, and H atoms and Stuttgart pseudopotentials for Mo atoms have been carried out for all species involved in the fragmentation processes depicted in eqs 1−6 described above. The dissociation processes of S_2 from $\mathbf{1a}^{-}$ and $\mathbf{2}^{2-}$ clusters are

(37) (a) Meienberger, M. D.; Hegetschweiler, K.; Rüegger, H. *Inorg. Chim. Acta* **1993**, *213*, 157. (b) Sokolov, M. N.; Abramov, P. A.; Gushchin, A. L.; Kalinina, I. V.; Naumov, D. Y.; Virovets, A. V.; Peresypkina, E. V.; Vicent, C.; Llusar, R.; Fedin, V. P. *Inorg. Chem.* **2005**, *44*, 8116.

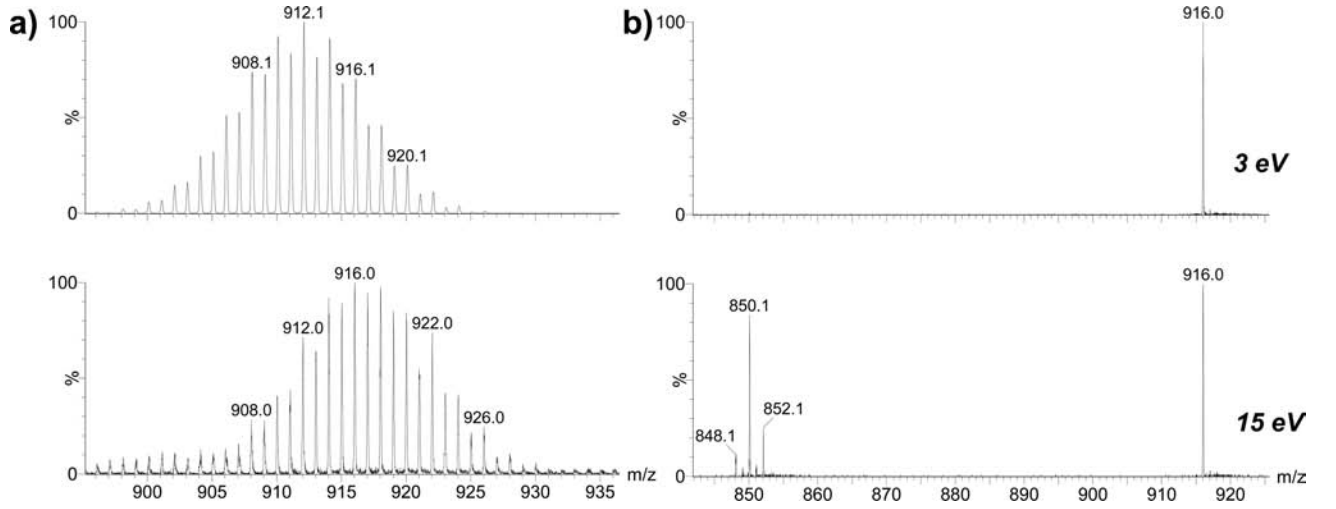

Figure 3. (a) Simulated isotopic pattern for $[Mo_3S_7Br_5]^-$ (top) and the observed peak for the ^{34}S enriched $[Mo_3S_7Br_5]^-$ anion (bottom) generated by treatment of $[Mo_3S_7Br_6]^{2-}$ and $^{34}SPPh_3$; (b) CID mass spectra of the ^{34}S enriched $[Mo_3S_7Br_5]^-$ anion (m/z = 916.0) at E_{lab} = 3 and 15 eV.

discussed jointly for a better comparison while the loss of the bdt molecule observed for the $\mathbf{2a}^{2-}$ cluster is analyzed separately. These fragmentations (eq 3−5) cannot be described by a single step, and reaction pathways leading to a structure in which the observed fragments are ready to be dissociated have to be elucidated. The stationary points along these pathways are labeled by the corresponding parent compound, $\mathbf{1a}^-$ (eq 3), $\mathbf{2}^{2-}$ (eq 4), and $\mathbf{2a}^{2-}$ (eq 5), followed by a number (for minima) or by the symbol TS (for the transition structures connecting minima), and the total charge of the structure.

Loss of Br^- from $\mathbf{1}^{2-}$. The heterolytic rupture of one Mo−Br bond in the $\mathbf{1}^{2-}$ dianion (eq 2) renders the unsaturated anion $[Mo_3S_7Br_5]^-$ ($\mathbf{1a}^-$) whose structure is represented in Figure 4. Although there are two non-equivalent bromine atoms (those located trans and cis to the μ_3S atom), the same $\mathbf{1a}^-$ cluster is obtained upon full geometry optimization irrespective of the removed bromine. The sum of the energy of the dissociated fragments ($\mathbf{1a}^-$ and Br^-) is 9.6 kcal mol^{-1} below the $\mathbf{1}^{2-}$ dianion pointing out the strong tendency of bromine anion to be lost, as evidenced in the ESI mass spectrum with the presence of significant abundances (ca. 40%) of the $\mathbf{1a}^-$. Coulomb repulsion in this doubly charged $\mathbf{1}^{2-}$ species may also contribute to the observed charge splitting process.[38] Removal of this bromine is not associated to large variations in the main geometric features within the Mo_3S_7 cluster core as compared with $\mathbf{1}^{2-}$. The only significant geometric difference between $\mathbf{1}^{2-}$ and $\mathbf{1a}^-$ clusters is related to the relative disposition of the terminal bromine group attached to the unsaturated metal site, which in $\mathbf{1a}^-$ appears located trans to the μ_3-S capping sulfur atom leading to a rare pseudooctahedral unsaturated molybdenum site (see Figure 4).

Loss of S_2 from $\mathbf{1a}^-$ and $\mathbf{2}^{2-}$ Clusters. There are three different types of sulfur atoms in $\mathbf{1a}^-$ and $\mathbf{2a}^{2-}$ clusters (capping, equatorial and axial), which could be released upon fragmentation, opening a very large number of possible fragmentation pathways to be explored. However, on the basis of ^{34}S isotopically labeling experiments detailed in the previous section, only equatorial sulfur atoms are released

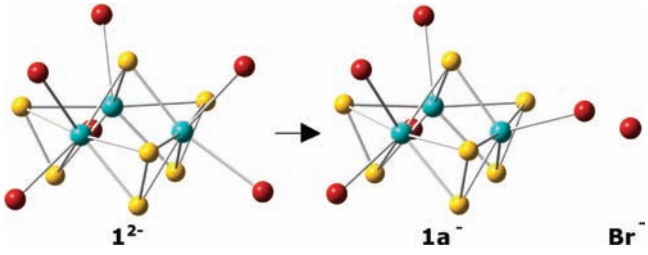

Figure 4. Geometrical representation of the DFT optimized structures for the fragmentation process of $\mathbf{1}^{2-}$ into $\mathbf{1a}^-$ plus $\mathbf{Br}^-$. Mo−Mo bonds are not displayed for clarity.

for the formation of S_2. Therefore, the species $\mathbf{1b}^-$ and $\mathbf{2a}^{2-}$ are proposed by removal of two S_{eq} (see Figure 5).

Since the $\mathbf{1a}^-$ product ion possesses C_s symmetry, there are two types of S_{eq} atoms: (i) S7 and S8, attached to the unsaturated Mo1, and (ii) S9 (see Figure 5 for numbering of involved atoms). Consequently, two possible reaction paths starting from the $\mathbf{1a}^-$ intermediate should be considered to account for the loss of S_2 from equatorial sulfur atoms. Similar energy differences were obtained when S7 and S8 or S7 and S9 were removed. The cluster $\mathbf{2}^{2-}$ possess C_{3v} symmetry; consequently all S_{eq} atoms are equivalent, and there is only one possible pathway leading to structure $\mathbf{2a}^{2-}$ (see Supporting Information, Figure S4). The DFT calculated fragmentation energies for eq 3 and 4 are 19.9 and 6.3 kcal mol^{-1}, respectively. The ground state ($^3\Sigma_g^-$) for the S_2 molecule has been considered. The main geometrical parameters within the Mo_3 cluster core do not change significantly upon removal of the two S_{eq} atoms.

The characterization of the fragmentation pathways eqs 3 and 4 are not straightforward, and a stepwise molecular mechanism allowing the formation of the S_2 molecule interacting weakly with the clusters $\mathbf{1b}^-$ and $\mathbf{2a}^{2-}$ has to be determined for $\mathbf{1a}^-$ and $\mathbf{2}^{2-}$ structures. Previous studies suggested a concerted mechanism in which the reaction coordinate is defined by opening of the angle $S_{eq}-S_{ax}-S_{capping}$ for two S_{eq} atoms moving simultaneously.[35] All attempts to find theoretically a concerted pathway were unsuccessful, and a stepwise mechanism based on the sequential opening of the $S_{eq}-S_{ax}-S_{capping}$ angles for two S_{eq} atoms has been

(38) Schröder, D. *Angew. Chem., Int. Ed.* **2004**, *43*, 1329.

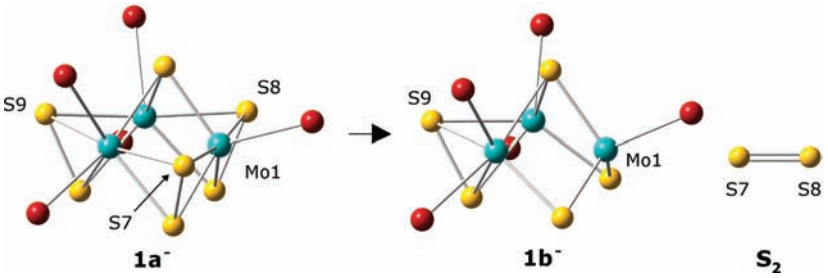

Figure 5. Geometrical representation of the DFT optimized structures for the fragmentation process of $\mathbf{1a}^-$ into $\mathbf{1b}^-$ plus S_2. Mo−Mo bonds are not displayed for clarity.

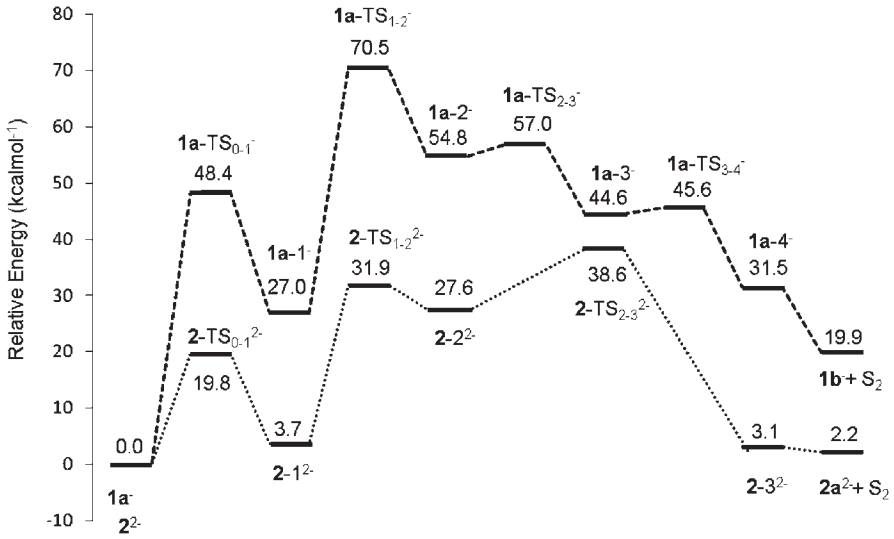

Figure 6. Energetic profile calculated at the DFT level for the fragmentation mechanism from $\mathbf{1a}^-$ and $\mathbf{2}^{2-}$ clusters to $\mathbf{1b}^- + S_2$ (dashed line) and $\mathbf{2a}^{2-} + S_2$ (dotted line). Energies relative to the corresponding parent compound (in kcal mol^{-1}).

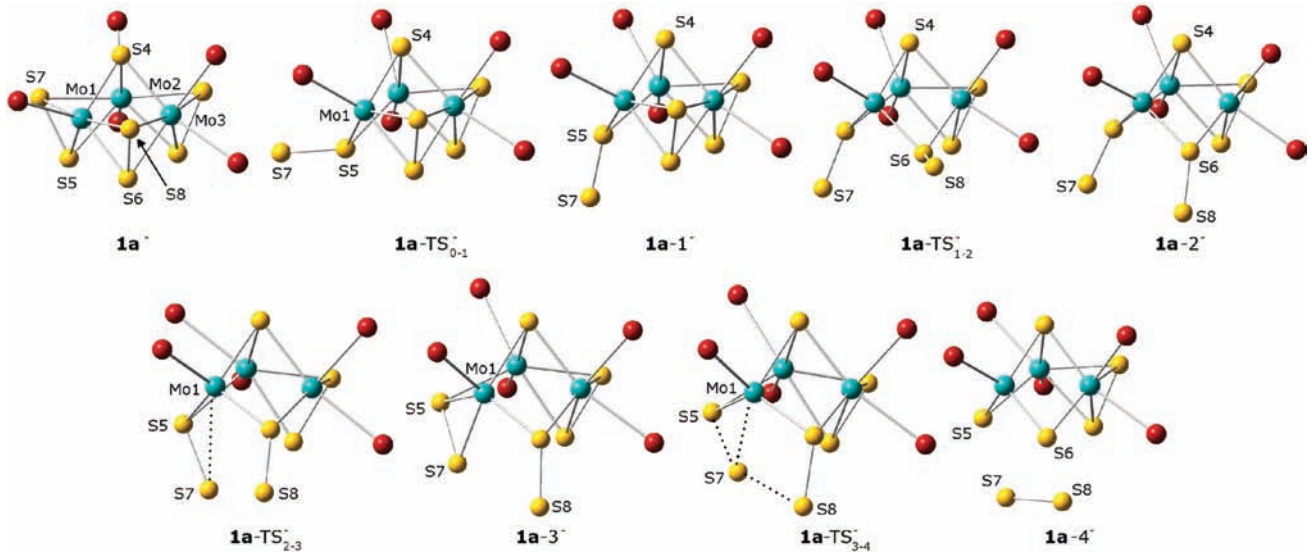

Figure 7. Geometrical representation of the DFT optimized structures for all stationary points along the fragmentation process of $\mathbf{1a}^-$ into $\mathbf{1a}$-4^-. Mo−Mo bonds are not displayed for clarity.

determined. Because of the large computational cost, the bdt ligands have been replaced by the model $S_2C_2H_2$ group. The computed energetic profiles of the fragmentation reaction evolving S_2 for the $\mathbf{1a}^-$ and $\mathbf{2}^{2-}$ dianions are shown in Figure 6 while the optimized geometries for all species along the reaction paths are represented in Figures 7 and 8. Thermochemical data for all species are reported in the Supporting Information.

The ligands (Br and bdt) coordinated to the Mo centers outside the Mo_3S_7 cluster core do not participate in the mechanism, therefore both clusters ($\mathbf{1a}^-$ and $\mathbf{2}^{2-}$) share the same elementary steps for the loss of two

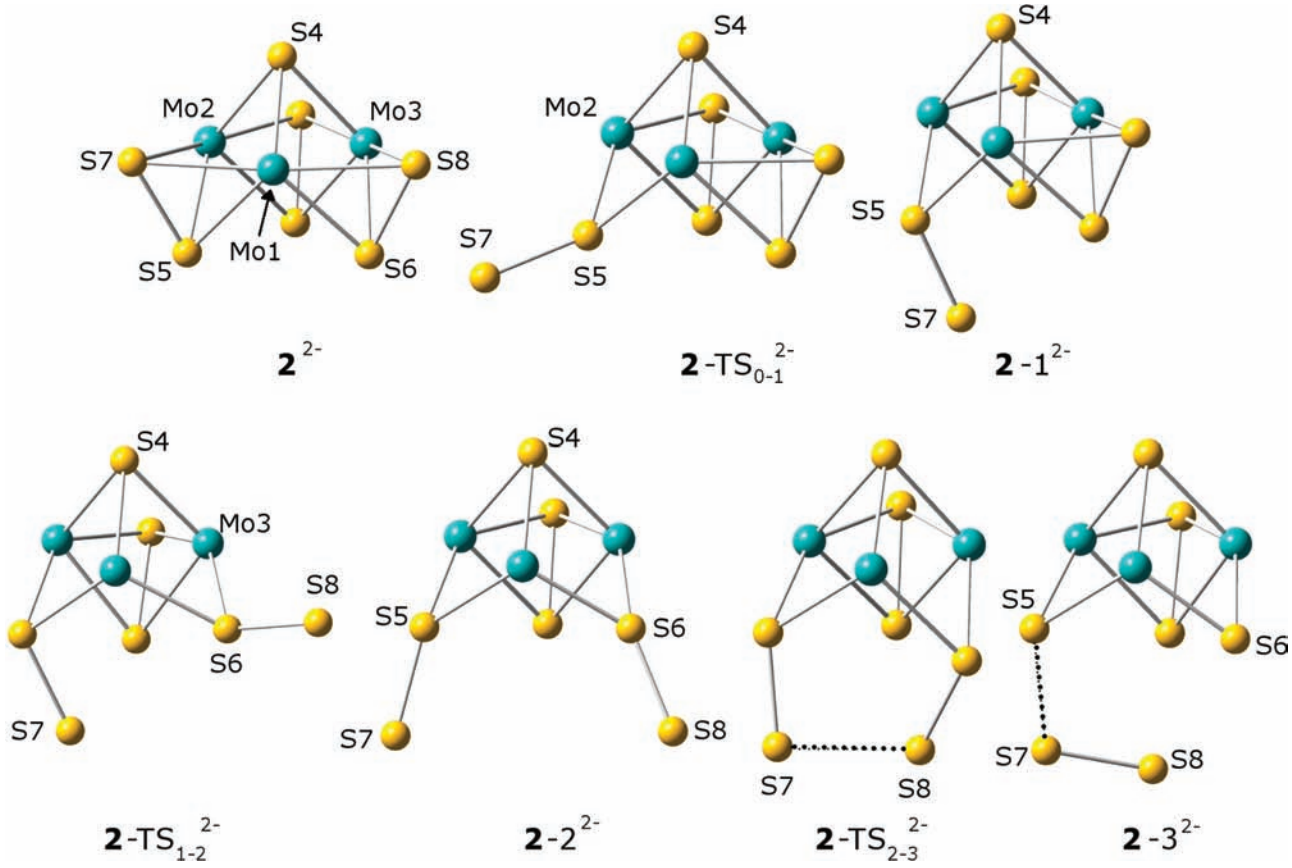

Figure 8. Geometrical representation of the DFT optimized structures for all stationary points along the fragmentation process of $\mathbf{2}^{2-}$ into **2**-3^{2-}. Mo−Mo bonds and dithiolene ligands on Mo atoms are not displayed for clarity.

S_{eq} into S_2. The only difference is that the unsaturated Mo of cluster $\mathbf{1a}^-$ allows the formation of an intermediate which is not present in the reaction mechanism of cluster $\mathbf{2}^{2-}$. The angle S7−S5−S4 (see Figures 7 and 8) at the starting structure equals 57.5° and 60.0°. The process starts with the rotation of S7 atom around the S5 atom, breaking both Mo1−S7 and Mo2−S7 bonds via a transition state with an energy barrier of 48.4 and 19.8 kcal mol^{-1}, **1a**-TS_{0-1}^- and **2**-$TS_{0-1}{}^{2-}$, being the angle S4−S5−S7 of 125.2° and 139.2° and characterized by one imaginary frequency of 387.2i and 178.7i cm^{-1}, respectively. The mode corresponding to the imaginary frequencies can be described as to Mo1−S7 and Mo2−S7 bond stretching and also umbrella inversion at the S5 atom.

Intermediates **1a**-1^- and **2**-1^{2-} are located 27.0 and 3.7 kcal mol^{-1} above the parent compound respectively, and S7 is now a terminal atom with considerable partial charges of −0.186e (**1a**-1^-) and −0.335e (**2**-1^{2-}). The second S_{eq} atom follows a similar process by breaking the Mo2−S8 and Mo3−S8 bonds via **1a**-TS_{1-2}^- and **2**-$TS_{1-2}{}^{2-}$ located 70.5 and 31.9 kcal mol^{-1} above the respective parent compounds and presenting similar geometrical and vibrational features to the previous transition structures. An intermediate, labeled **1a**-2^- and **2**-2^{2-}, is found with relative energies of 54.8 and 27.6 kcal mol^{-1}, respectively. This structure presents two terminal sulfur atoms (S7 and S8) carrying partial negative charges of −0.147e (S7) and −0.147e (S8) for cluster **1a**-2^- and −0.303 (S7) and −0.298 (S8) for cluster **2**-2^{2-}.

Comparison of the energetic profiles (see Figure 6) for the transformation of equatorial sulfur atoms into terminal ones reveals that the process for $\mathbf{1a}^-$ cluster is more energetically demanding than for $\mathbf{2}^{2-}$ cluster. This can be explained by the total charge of the cluster; the excess of negative charge stabilizes the formation of terminal sulfur atoms and facilitates the process.

The following step is the bond formation between terminal sulfur atoms (S7 and S8) and the concomitant rupture of two $S_{axial}-S_{eq}$ bonds. Because of the vacancy at Mo1 in the $\mathbf{1a}^-$ cluster, a new intermediate (**1a**-3^-) appears via a low energy barrier (**1a**-TS_{2-3}^-, 57.0 kcal mol^{-1}, 106.1i cm^{-1}) in which the S7 atom is bonded to Mo1 and S5, lying 44.6 kcal mol^{-1} above $\mathbf{1a}^-$. In a second step, a transition structure corresponding to the S7−S8 bond formation is found, **1a**-TS_{3-4}^- at 45.6 kcal mol^{-1}, being characterized by one imaginary frequency 115.5i cm^{-1} and a S7−S8 distance of 2.777 Å. For the $\mathbf{2}^{2-}$ cluster, the formation of the S7−S8 bond from **2**-2^{2-} occurs via a single step, the **2**-$TS_{2-3}{}^{2-}$ structure which is found at 38.6 kcal mol^{-1} for a S7−S8 intranuclear distance of 2.679 Å, displaying one imaginary frequency of −246.3i cm^{-1} associated mainly to the S7−S8 bond stretching. The resulting structures, **1a**-4^- and **2**-3^{2-} correspond to the $\mathbf{1b}^-$ and $\mathbf{2a}^{2-}$ clusters, respectively, forming intramolecular adducts with the S_2 molecule which are dissociated.

Formation of the $\mathbf{1b}^-$ and $\mathbf{2a}^{2-}$ species represents a formal reduction of two bridging disulfide ligands through an internal two-electron redox process to give two sulfide ligands

and a molecule of S_2 according to eqs 8 and 9:

$$[Mo_3(\mu_3\text{-}S)(\mu\text{-}S_2)(\boldsymbol{\mu\text{-}S_2})_2Br_5]^- \ (\mathbf{1a}^-)$$
$$\rightarrow [Mo_3(\mu_3\text{-}S)(\mu\text{-}S_2)(\boldsymbol{\mu\text{-}S})_2Br_5]^- \ (\mathbf{1b}^-) + \mathbf{S_2} \quad (8)$$

$$\textit{overall reaction} \qquad 2S_2^{2-} \rightarrow 2S^{2-} + S_2$$

$$[Mo_3(\mu_3\text{-}S)(\mu\text{-}S_2)(\boldsymbol{\mu\text{-}S_2})_2(bdt)_3]^{2-} \ (\mathbf{2}^{2-})$$
$$\rightarrow [Mo_3(\mu_3\text{-}S)(\mu\text{-}S_2)(\boldsymbol{\mu\text{-}S})_2(bdt)_3]^{2-} \ (\mathbf{2a}^{2-}) + \mathbf{S_2} \quad (9)$$

$$\textit{overall reaction} \qquad 2S_2^{2-} \rightarrow 2S^{2-} + S_2$$

For comparative purposes, we also investigate theoretically the abstraction of S_2 from two equatorial positions with respect to a hypothetical disulfide $S_{ax}-S_{eq}$ abstraction (see Supporting Information, Figure S5). The former process is energetically favored to give the product $\mathbf{1b}^-$ lying only 19.9 kcal mol^{-1} higher in energy than $\mathbf{1a}^-$, whereas the loss of one bridging disulfide yields the cluster $\mathbf{1c}^-$ which is 62.2 kcal mol^{-1} above $\mathbf{1a}^-$. Hence, the proposed fragmentation channel agrees with the isotopic labeling experiments as well as the selective chalcogen exchange experiments described above where the equatorial-chalcogen (Q_{eq}) atoms are more prone to be released. On the basis of the molecular structure of the $\mathbf{1c}^-$ anions, its formation would correspond to the internally induced disulfide to S_2 oxidation and the concomitant metal reduction. Analogous reactions triggered by external oxidants are ubiquitous in mono- and dinuclear group 6 chalcogenide chemistry,[5,6,39] although they have not been observed for their trinuclear counterparts.

Loss of bdt from $\mathbf{2a}^{2-}$ Cluster. The cluster $\mathbf{2a}^{2-}$ presents two non-equivalent molybdenum atoms, those bridged by the disulfide ligand or that located far from disulfide-bridged ligand. Consequently, two different dithiolene ligands are prone to be dissociated. Fragmentation of bdt without participation of the disulfide bridge would represent an internally induced bdt^{2-} to bdt oxidation and the concomitant metal reduction. However, theoretical calculations on the possible species upon release of the bdt ligand, $\mathbf{2b}^{2-}$ (that evolving the bdt ligand close to the disulfide bridge) and $\mathbf{2c}^{2-}$ (that evolving the bdt ligand far from the disulfide bridge), reveal very different stability and participation of the disulfide ligand. Hence, the fragmentation reaction of species $\mathbf{2a}^{2-}$ to yield $\mathbf{2b}^{2-}$ plus bdt (32.2 kcal mol^{-1}) involves chemical transformation of a S_2^{2-} ligand to one sulfide and one terminal sulfur ligand (see Figure 9) and is thermodynamically favored over that fragmentation reaction affording $\mathbf{2c}^{2-}$ in which the disulfide ligand remains intact (102.8 kcal mol^{-1}). Experimental evidence supporting that $\mathbf{2b}^{2-}$ is the resulting specie of the fragmentation of $\mathbf{2a}^{2-}$ comes from the absence of fragmentation of $\mathbf{3}^{2-}$ because of the lack of equatorial S atoms which facilitate somehow the release of bdt. Therefore, to explain how the disulfide ligand assists the departure of the bdt ligand, a low energy possible fragmentation pathway from $\mathbf{2a}^{2-}$ to $\mathbf{2b}^{2-}$ has been theoretically determined (Figure 10).

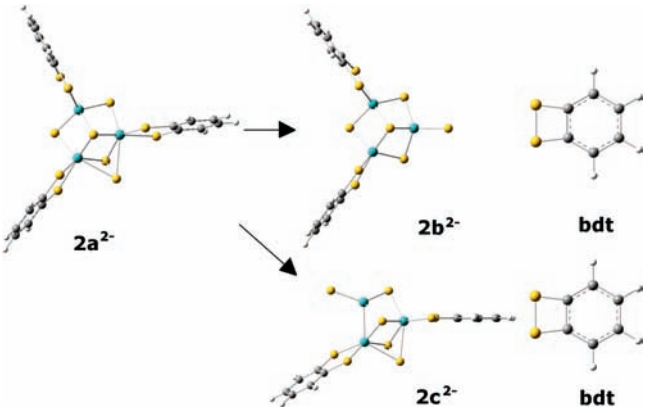

Figure 9. Geometrical representation of the DFT optimized structures for the fragmentation process of $\mathbf{2a}^{2-}$ into $\mathbf{2b}^{2-}$ plus bdt or into $\mathbf{2c}^{2-}$ plus bdt. Mo−Mo bonds are not displayed for clarity.

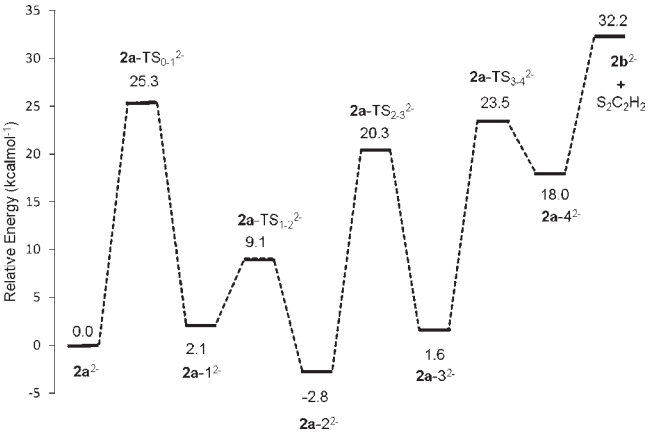

Figure 10. Energetic profile calculated at DFT level for the fragmentation mechanism from $\mathbf{2a}^{2-}$ cluster to $\mathbf{2b}^{2-}$ plus $S_2C_2H_2$. Energies relative to the corresponding parent compound (in kcal mol^{-1}).

The process taking place can be related to the proposed redox isomerism where a trithiolene structure has been postulated on the basis of experimental findings.[4,7,40] The corresponding trithiolene specie is 2.8 kcal mol^{-1} more stable than the starting cluster $\mathbf{2a}^{2-}$. Therefore, a stepwise reaction mechanism is proposed and determined theoretically (see Figure 11 for atom numbering) considering the trithiolene intermediate. The basic steps can be described as follows: (i) migration of the equatorial sulfur atom (S10) taking part of a bidentate disulfide ligand to a metal-dithiolene bond (Mo2−S11), (ii) insertion of S10 into the Mo2−S11 bond leading to the trithiolene intermediate, and (iii) breaking of the S10−S11 and Mo2−S12 bonds and formation of a terminal sulfide ligand accompanied by release of a neutral dithiolene ligand. This mechanism can be regarded as a formal two-electron reduction of one bridging S_2^{2-} ligand to give one bridged and one terminal sulfide (S^{2-}) ligands and the concomitant oxidation of the dithiolene ligand, thus corresponding to the

(39) Sugimoto, H.; Tajima, R.; Sakurai, T.; Ohi, H.; Miyake, H.; Itoh, S.; Tsukube, H. *Angew. Chem., Int. Ed.* **2006**, *45*, 3520.

(40) Pilato, R. S.; Eriksen, K. A.; Greaney, M. A.; Stiefel, E. A.; Goswami, S.; Kilpatrick, L.; Spiro, T. G.; Taylor, E. C.; Rheingold, A. L. *J. Am. Chem. Soc.* **1991**, *113*, 9372.

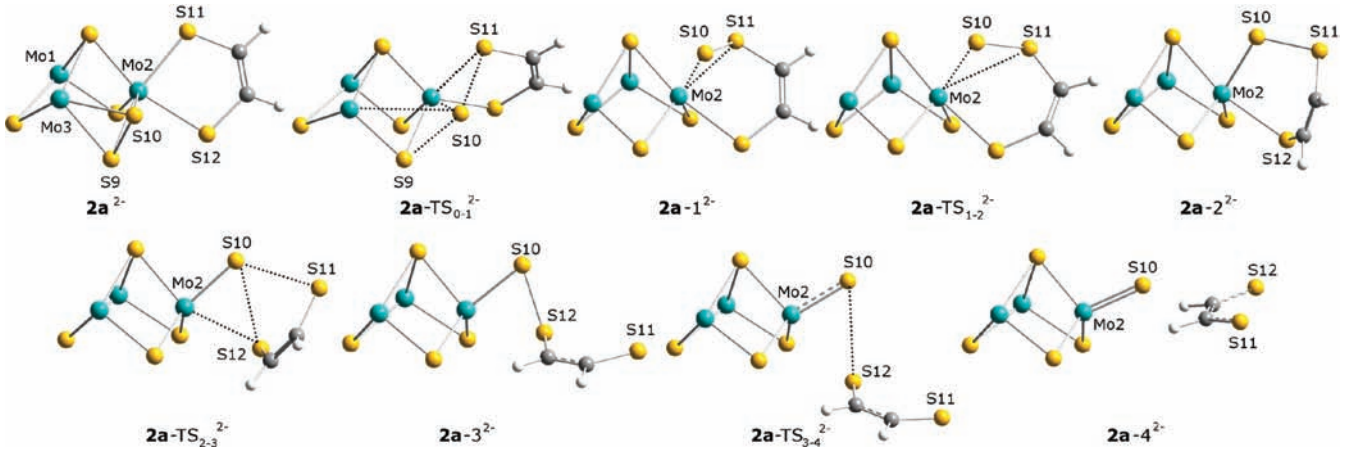

Figure 11. Geometrical representation of the DFT optimized structures for all stationary points along the fragmentation process of $\mathbf{2a}^{2-}$ into $\mathbf{2a}\text{-}4^{2-}$. Mo−Mo bonds and dithiolene ligands on Mo1 and Mo3 atoms are not displayed for clarity.

following ligand-based redox reaction 10.

$$[Mo_3(\mu_3\text{-}S)(\boldsymbol{\mu}\text{-}\mathbf{S_2})(\mu\text{-}S)_2(bdt)_2(\mathbf{bdt})]^{2-}\ (\mathbf{2a}^{2-}) \rightarrow [Mo_3(\mu_3\text{-}S)(\boldsymbol{\mu}\text{-}\mathbf{S})(\mathbf{S})(\mu\text{-}S)_2(bdt)_2]^{2-}\ (\mathbf{2b}^{2-}) + \mathbf{bdt} \quad (10)$$

$$\textit{overall reaction} \qquad bdt^{2-} + S_2{}^{2-} \rightarrow bdt + 2S^{2-}$$

At the $\mathbf{2a}^{2-}$ structure the equatorial sulfur (S10) takes part in a disulfide bridge (distance S10−S9 of 2.103 Å) between Mo2 and Mo3 atoms (distances S10−Mo2 and S10−Mo3 of 2.582 Å), and it is located far from the dithiolene ligand attached to Mo2 (S10−S11 distance 3.943 Å). However, the dithiolene is not totally rigid, and it can be rotated to a moderate extent. A transition structure is found for the migration of the S10 atom from the equatorial position to the S11 atom with an energy barrier of 25.3 kcal mol^{-1} and one imaginary frequency of 217.0i cm^{-1}. The geometry of the $\mathbf{2a}\text{-}TS_{0-1}{}^{2-}$ reveals that the S10 is moving toward S11 (S9−S10 distance of 2.500 Å and S10−S11 distance of 2.386 Å), while the distance S10−Mo2 has been shortened to 2.364 Å. The intermediate $\mathbf{2a}\text{-}1^{2-}$ is found 2.1 kcal mol^{-1} above $\mathbf{2a}^{2-}$, and the Mo2 atom is coordinated to a disulfide group formed by S10 and S11. The $\mathbf{2a}\text{-}TS_{1-2}{}^{2-}$ structure (9.1 kcal mol^{-1}, 75.6i cm^{-1}) shifts the coordination mode of Mo2 from the disulfide group to the recently inserted S10 atom, leading to the trithiolene structure $\mathbf{2a}\text{-}2^{2-}$ situated at −2.8 kcal mol^{-1}. The departure of the dithiolene ligand is obtained by stepwise breaking of the S10−S11 and Mo2−S12 bonds. The $\mathbf{2a}\text{-}TS_{2-3}{}^{2-}$ (20.3 kcal mol^{-1}, 149.4i cm^{-1}) presents a S10−S11 distance of 3.093 Å and leads to $\mathbf{2a}\text{-}3^{2-}$ (1.6 kcal mol^{-1}). The second step is the decoordination of S12 from Mo2 which occurs via the $\mathbf{2a}\text{-}TS_{3-4}{}^{2-}$ structure (23.5 kcal mol^{-1}, 31.6i cm^{-1}) leading to the formation of a charge-transfer complex, $\mathbf{2a}\text{-}4^{2-}$, at 18.0 kcal mol^{-1} previous to the dissociation into the $\mathbf{2b}^{2-}$ cluster and the dithiolene ligand.

Loss of bdt from $\mathbf{3}^{2-}$ Cluster. Although the considered path involving the expulsion of neutral bdt is not experimentally observed for the $\mathbf{3}^{2-}$ dianion, it is also included with the purpose of providing a deeper understanding of the fragmentation process. Theoretical calculations allow calculating the bond interaction energy between the bdt group and the cluster core, explaining the lack of the fragmentation processes observed for the $\mathbf{3}^{2-}$ cluster according to eq 11. Hence, reaction 11 is strongly endothermic (122.5 kcal mol^{-1}) indicating that without the assistance of an equatorial sulfur atom, the fragmentation of the oxidized bdt ligand is unaffordable (see Supporting Information, Figure S6).

$$[Mo_3(\mu_3\text{-}S)(\mu\text{-}S)_3(bdt)_3]^{2-}\ (\mathbf{3}^{2-}) \rightarrow [Mo_3(\mu_3\text{-}S)(\mu\text{-}S)_3(bdt)_2]^{2-}\ (\mathbf{3a}^{2-}) + bdt \quad (11)$$

Conclusions

The combined use of ESI, ESI tandem mass spectrometry, and DFT calculations provides detailed mechanistic insights into the gas-phase generation and fragmentation reaction studies of the $\mathbf{1}^{2-}$, $\mathbf{2}^{2-}$, and $\mathbf{3}^{2-}$ dianions. In general, the dominant fragmentation paths involve liberation of neutral molecules (S_2 or bdt) associated to two-electron redox processes. Because of the intrinsic electrochemical and structural properties of the $\mathbf{1}^{2-}$, $\mathbf{2}^{2-}$, and $\mathbf{3}^{2-}$ dianions, these two-electron processes are based on the sulfur ligands, thus making $\mathbf{1}^{2-}$, $\mathbf{2}^{2-}$, and $\mathbf{3}^{2-}$ dianions prototypical models to investigate ligand-based redox transformations. Ligand-based redox chemistry has been rarely observed at the active site of a molybdenum enzime.[41] Although the data presented here have been gathered from gas-phase experiments, the results might reveal general trends that should be applicable for either enhancing or deterring the appearance of redox reactions in solution as follows:

(i) We have observed that the elimination of neutral S_2 from $\mathbf{1}^{2-}$ and $\mathbf{2}^{2-}$ dianions proceeds through simultaneous abstraction of equatorial sulfur atoms, even though the net charge and the identity of the outer ligands in the $\mathbf{1a}^{-}$ and $\mathbf{2}^{2-}$ dianions are different. In addition, they both involve ligand-based redox reactions sharing identical reaction mechanisms (see the energetic profiles in Figure 6). Identical gas-phase fragmentation has been experimentally observed for the cationic $[Mo_3Q_7(dtc)_3]^+$ (Q = S, Se; dtc = dithiocarbamate) complex,[35] thus suggesting an inherent

(41) George, G. N.; Costa, C.; Moura, J. J. G.; Moura, I. *J. Am. Chem. Soc.* **1999**, *121*, 2625.

loss of equatorial diatomic S_2 characteristic for the Mo_3S_7 clusters in the gas-phase. Analogous selective abstraction is observed for Mo_3S_7 complexes in the condensed phase using reducing agents such as cyanide, H_3PO_2, or phosphines.[19,42]

(ii) A parallelism between the gas-phase behavior and the electrochemical properties of dithiolene-containing $\mathbf{2}^{2-}$ and $\mathbf{3}^{2-}$ complexes is observed. As can be inferred from CID experiments, electron detachment process is a common fragmentation path to $\mathbf{2}^{2-}$ and $\mathbf{3}^{2-}$ dianions (that formally corresponds to the oxidation of the cluster core (eqs 6 and 7)). This behavior is not observed for the Br-containing $\mathbf{1}^{2-}$ dianion in which charge reduction proceeds via heterolytic Mo−Br cleavage. This experimental evidence correlates with the electrochemical behavior described above for these Mo_3S_7 and Mo_3S_4 complexes, clearly indicating that dithiolene ligands are crucial to provide oxidation activity in the Mo_3S_7 and Mo_3S_4 clusters while Mo centers do not participate in the electron transfer process.

(iii) The importance of disulfide ligands (S_2^{2-}) as electron reservoirs to trigger intracomplex redox reactions is also manifested by two distinctive fragmentations, expulsion of S_2, observed for $[Mo_3S_7Br_5]^-$ ($\mathbf{1a}^-$) and $[Mo_3S_7(bdt)_3]^{2-}$ ($\mathbf{2a}^{2-}$) clusters, and dissociation of a neutral bdt ligand from a Mo atom in $[Mo_3S_5(bdt)_3]^{2-}$ ($\mathbf{2a}^{2-}$) which requires the assistance of a neighboring disulfide ligand. Our results suggest the plausible involvement of trithiolene ligands as intermediates in the release of the dithiete bdt molecule.

(iv) We have observed that the presence of disulfide ligands in $\mathbf{2}^{2-}$ is crucial to promote bdt dissociation leading to the $[Mo_3S_5(bdt)_2]^{2-}$ species with terminal Mo=S groups. This process closely resembles the reverse step of the induced internal redox reaction between the tetrathiometalate MoS_4^{2-} or $MoS_2O_2^{2-}$ with bis(trifluoromethyl)-1,2-dithiete in which, remarkably, the starting materials are the product ions observed in the CID spectra of $\mathbf{2}^{2-}$. Equation 12 is quantitative and clean and affords the mononuclear dithiolene complexes $[Mo(1,2\text{-dithiolene})_3]^{2-}$ together with elemental sulfur (denoted as 4¨S¨);[6] however, the yield for eq 13 to afford compound $[Mo(O)(dithiolate)_2]^{2-}$ plus elemental sulfur (depicted as ¨S¨), is low and presumably the remaining oxo ligand (depicted as ¨O¨) is hydrolyzed or protonated by adventious water in the reaction media.[6]

$$[MoS_4]^{2-} + 3(\text{dithiete}) \rightarrow [Mo(\text{dithiolate})_3]^{2-} + 4{\cdot\cdot}S{\cdot\cdot} \quad (12)$$

$$[MoS_2O_2]^{2-} + 2(\text{dithiete}) \rightarrow [Mo(O)(\text{dithiolate})_2]^{2-} + {\cdot\cdot}S{\cdot\cdot} + {\cdot\cdot}O{\cdot\cdot} \quad (13)$$

The overall reactions 12 and 13 are complex since they involve simultaneous metal and dithiete reduction along with sulfur oxidation, and the identification of reaction intermediates remains unknown. However, it can be reasonably assumed that reactions 12 and 13 are triggered by initial dithiete coordination to the Mo site containing the Mo=S functional group. If one adopts the generalized reaction $bdt^{2-} + S_2^{2-} \rightarrow bdt + 2S^{2-}$ (eq 10) described in detail above, we hypothesize that the first step of the reaction showed in reactions 12 and 13 corresponds to the oxidation of two sulfide ligands accompanied by the reduction and coordination of the dithiolene ligand.

Acknowledgment. The financial support of the Spanish Ministerio de Ciencia e Innovación (Grants CTQ2008-02670 and CTQ2009-14629-C02-02), Fundació Bancaixa-UJI (research project P1.1B2007-12), Generalitat Valenciana (ACOMP/2010/276 and Prometeo/2009/053) is gratefully acknowledged. Prof. V. Fedin is acknowledged for providing us the ^{34}S-enriched sample of elemental sulfur. The authors also thank the Servei Central d'Instrumentació Cientifica (SCIC) of the Universitat Jaume I for providing us with the mass spectrometry and X-ray facilities. The authors also are grateful to the Servei d'Informatica, Universitat Jaume I for generous allotment of computer time.

Supporting Information Available: Complete reference for Gaussian 03; Cyclic voltammogram and ORTEP representation of the $\mathbf{3}^{2-}$ dianion, CID spectra of the $[Mo_3S_3Se_3Br_6]^{2-}$ dianion; geometrical representation of the DFT optimized structures for the fragmentation process of $\mathbf{2}^{2-}$ to $\mathbf{2a}^{2-}$ plus S_2, $\mathbf{1a}^-$ into $\mathbf{1c}^-$ plus S_2, geometrical representation of the DFT optimized structures for the fragmentation process of $\mathbf{3}^{2-}$ into $\mathbf{3a}^{2-}$ plus bdt and thermochemical data calculated at B3LYP level for all species. Crystallographic data (excluding structure factors) for the structures reported in this paper. This material is available free of charge via the Internet at http://pubs.acs.org.

(42) Fedin, V. P.; Sykes, A. G. *Inorg. Synth.* **2001**, *33*, 162.